



Dielectric and electrical characterization of lead-free complex electronic ceramic: $(\text{Bi}_{1/2}\text{Li}_{1/2})(\text{Zn}_{1/2}\text{W}_{1/2})\text{O}_3$

T. Mahapatra¹ · S. Halder¹ · S. Bhuyan¹ · R. N. P. Choudhary²

Received: 2 March 2018 / Accepted: 4 September 2018 / Published online: 6 September 2018
© Springer Science+Business Media, LLC, part of Springer Nature 2018

Abstract

A Lead-free complex perovskite compound of $(\text{Bi}_{1/2}\text{Li}_{1/2})(\text{Zn}_{1/2}\text{W}_{1/2})\text{O}_3$ has been synthesized by using high-temperature solid-state reaction technique. The structural, micro-structural, dielectric constant, tangent loss, electrical impedance, modulus, conductivity and polarization characteristics of the prepared compound have been studied over a wide range of temperature (150–500 °C) and frequency (1 kHz–1 MHz). The X-ray diffraction structural analysis reveals tetragonal structure of the compound with cell parameters; $a = 10.6055$ (36) Å, $c = 13.8275$ (36) Å, $c/a = 1.3038$ and volume $V = 1555.27$ Å³. The acquired room temperature scanning electron micrograph exhibits the homogeneous distribution of fibre-type of grains throughout the surface of specimen. The dielectric constant and tangent loss of the material at a frequency of 1 kHz are found to be 4000 and 11 respectively. The ac conductivity spectrum provides the information about the conduction mechanism and semiconducting nature of the compound. The impedance spectrum provides an insight into the contributions of grain and grain boundary effects in the resistive and capacitive characteristics of the materials. The frequency dependence of complex modulus analysis shows the presence of non-Debye type of relaxation behaviour in the material.

1 Introduction

Recent studies of a large number of materials of different structural families have shown that some ceramic materials with perovskite structure have a high dielectric constant and low tangent loss which are useful for device applications including dielectric resonators [1–3]. Nowadays, these dielectric resonators are used in filters, oscillators, cellular phones, etc. Previously, in most of the industrial applications, Lead (Pb)-based perovskite materials (generally ABO_3 type: A = mono or divalent ions, B = tri to hexavalent ions) have been widely used due to their enhanced physical properties. Nowadays, they are replaced by non-Lead based compounds to limit their hazardous impact on both environment and human being. The manufacturing and machine wastes of Lead-based materials cause lots of pollution, and hence cannot be easily recycled. Therefore, the researchers have

led their interest for formulation of Lead-free electroceramic materials which is eco-friendly with high humidity sensitive electrical properties comparable to those of Pb-based ones. Some Bismuth (Bi)-based perovskite materials have attracted much interest of researchers due to their low toxic nature, low sintering temperature and good ionic conductivity at a temperature above 730 °C. Multiferroics are some special class of materials that show both ferroelectric and ferromagnetic properties due to which these compounds have potential applications in actuators, resonators, filters, sensors, phase shifters etc. Out of all perovskite multiferroic compounds Bismuth based material BFO (BiFeO_3) is one of the promising candidate due to its high Neel and ferroelectric Curie temperature. But due to its limitation including lack of structural distortion, leakage current, electrical conductivity, impurity phase formation, it has been restricted for various applications [4–6]. Some Lithium-based materials are now emerging as an important material in modern society due to their wide-scale use in various energy storage devices. In view of the importance of the materials for applications [7–11], an attempt has been made to synthesize a Lead-free multiferroic material with enhanced physical properties and less limitations that can meet the demand of present and future industrial applications [12, 13] by partially replacing the Bi of BFO by Lithium (Li) and completely replacing Fe

✉ S. Halder
sarbasrihalder@gmail.com

¹ Department of Electronic and Communication Engineering, Siksha 'O' Anusandhan (Deemed to be University), Bhubaneswar 751030, India

² Department of Physics, ITER, Siksha 'O' Anusandhan (Deemed to be University), Bhubaneswar 751030, India

by Zinc (Zn) and Tungsten (W) to form a perovskite type of structure. In the present study, therefore, it has been tried to fabricate a multiferroic compound with a complex chemical composition of perovskite structure, $(\text{Bi}_{1/2}\text{Li}_{1/2})(\text{Zn}_{1/2}\text{W}_{1/2})\text{O}_3$ (BLZWO), using non-toxic inorganic oxides at high temperatures. Based on the extensive literature survey, it is concluded that no work is reported regarding this compound so far to the best of our knowledge. Therefore, in the current article, the structural, dielectric and electrical properties of the material using different characterization techniques and experimental conditions have been reported.

2 Experimental procedure

The polycrystalline sample of $(\text{Bi}_{1/2}\text{Li}_{1/2})(\text{Zn}_{1/2}\text{W}_{1/2})\text{O}_3$ (BLZWO) is prepared using the high-purity (> 99.5% purity) oxide powders of Bismuth trioxide (Bi_2O_3), Lithium carbonate (Li_2CO_3), Zinc oxide (ZnO) and Tungsten trioxide (WO_3) (all from M/S LOBA Chemical, India) by a mixed oxide (high-temperature solid-state reaction) technique. To fabricate the compound, the above powders are weighted in stoichiometric amount by using a high-precision digital electronic balance (Mettler Type: New Classic MF; Model: ML204/A01). Then the powders of the raw materials are mixed by dry grinding followed by wet grinding using agate motor and pestle. The uniformly mixed powder is then calcined at an optimized temperature of 750 °C for 4 h in a high-temperature furnace. To affirm the formation of synthesized sample, the calcined powder was checked using X-ray diffraction (XRD) data and pattern. The homogenized mixture of powders after calcinations is undergone for re-milling to prepare fine powder, and then by mixing polyvinyl alcohol (PVA) as a binder which is pressed into disc shaped pellets by a hydraulic press at an iso-static pressure of $4 \times 10^6 \text{ Nm}^{-2}$. The disk-shaped specimens are sintered at 750 °C by placing them in a boat for 4 h in a furnace. A sintered pellet is then electroded with highly-conducting silver paint (M/S Sigma-Aldrich) to measure its electrical properties. The basic structural parameters of $(\text{Bi}_{1/2}\text{Li}_{1/2})(\text{Zn}_{1/2}\text{W}_{1/2})\text{O}_3$ is determined using diffraction data obtained from X-ray diffractometer for Bragg angle ($20 \leq 2\theta \leq 80$) at a scanning rate of $3^\circ/\text{min}$. The possible structure of the compound is determined by indexing all the peaks of the X-ray diffraction (XRD) pattern using a powder diffraction data analyser software program ‘POWDMULT’ (version 2.2). The morphological structure of the ceramic sample (pellet) is studied using a scanning electron microscope. For measuring the various electrical parameters (impedance, loss tangent, capacitance, etc) and dielectric parameters, a computer-controlled impedance meter (PSM 4NL; Model 1735, UK) has been used over a wider range of frequency (10^3 – 10^6 Hz) and temperature (25–500 °C). This phase sensitive LCR meter is connected

to a vertical pit furnace and laboratory fabricated sample holder. To record the temperature, a digital milli-voltmeter (KUSAM MECO 108) and a chromel–alumel thermocouple has been used.

3 Results and discussion

3.1 Structural study

X-ray diffraction technique is used to obtain the structural data of the sintered specimen. Figure 1 shows X-ray powder reflection pattern of the studied compound (BLZWO) at room temperature. The diffraction peaks of the synthesized compound do not match with those of ingredients of the fabricated sample [14]. The sharp diffraction peaks are well indexed in a particular (tetragonal) crystal system by POWD software [15, 16]. It is confirmed that the structure of the compound is of a distorted perovskite type, and the refined lattice parameters (using least-squares refinement sub-routine) of the material are: $a = 10.6055$ (36) Å, $c = 13.8275$ (36) Å, $c/a = 1.3038$ and volume $V = 1555.27$ Å³ (figure in parenthesis of cell parameters is estimated standard deviation). The crystallite size of the fabricated sample is estimated using the Scherrer’s equation for a particular reflection hkl as: $P_{hkl} = k \lambda / (\beta_{1/2} \cos\theta)$ [17] where $\lambda = 1.5405$ Å, k (constant) = 0.89, and $\beta_{1/2}$ = full width at half maximum (in radians). The average crystallite size P is found to be 84 ± 5 nm.

The tolerance factor, referred as Goldschmidt tolerance factor (T), is one of the important criteria that provides information about the stability and distortion of the crystal structure. It is defined as $T = \frac{r_A + r_o}{\sqrt{2}(r_B + r_o)}$, where r_A and r_B are ionic radius of A and B site atoms and r_o is the ionic radius

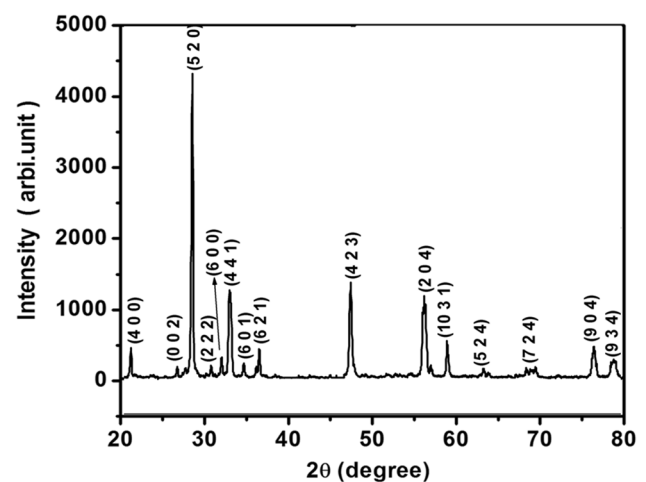


Fig. 1 Room temperature XRD pattern of $(\text{Bi}_{1/2}\text{Li}_{1/2})(\text{Zn}_{1/2}\text{W}_{1/2})\text{O}_3$

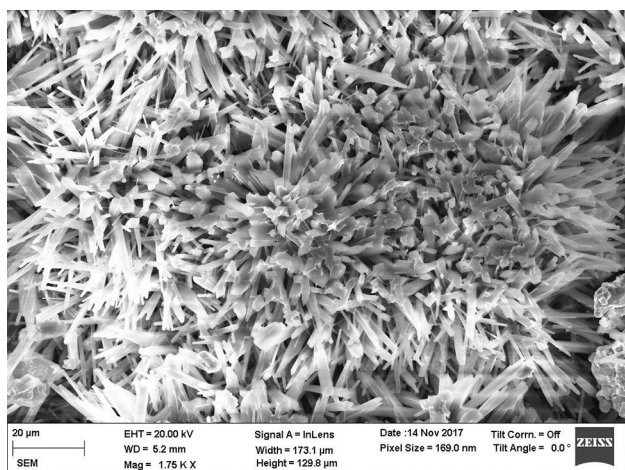


Fig. 2 SEM image of $(\text{Bi}_{1/2}\text{Li}_{1/2})(\text{Zn}_{1/2}\text{W}_{1/2})\text{O}_3$

of O^{2-} . For an ideal perovskite structure, the tolerance factor is 1. If tolerance factor is closer to one, then the structure of the compound is indicated as stable (normal) in an ideal perovskite. The calculated value of T of the studied compound is found to be 0.7 that is far away from a normal perovskite, hence this compound is found to be less stable with distorted structure.

Figure 2 displays the microstructure of the BLZW pellet using scanning electron microscope (SEM). The careful examination of SEM pattern shows a unique flower-like dense microstructure of the studied compound with uniform distribution of grains.

3.2 Dielectric study

In recent years, study of dielectric properties of the materials plays an important role due to their practical applications in microelectronics and optoelectronic fields [18–20]. Figure 3a, b illustrate the frequency dependence of relative dielectric constant (ϵ_r) and dissipation factor [tangent loss ($\tan\delta$)] of the studied (BLZWO) compound at selected temperatures. It is clear from the plots that with rise in frequency, both ϵ_r and $\tan\delta$, decrease (i.e., they are inversely proportional to frequency) which is a general trend of dielectrics that can be well understood by polarisation mechanism [21]. The polarization is created in the materials due to the electronic exchange of the number of ions by locally displacing the electrons in the applied field direction. At low frequencies, there is a charge accumulation at the interface, and hence the contributions of different polarizations (interfacial, atomic, ionic dipolar, and electronic polarizations) are observed. It is the main reason for rising of dielectric constant on decreasing frequency. The dielectric constant decreases with rise in frequency. The reason behind this trend is that at a certain point, the space charges cannot

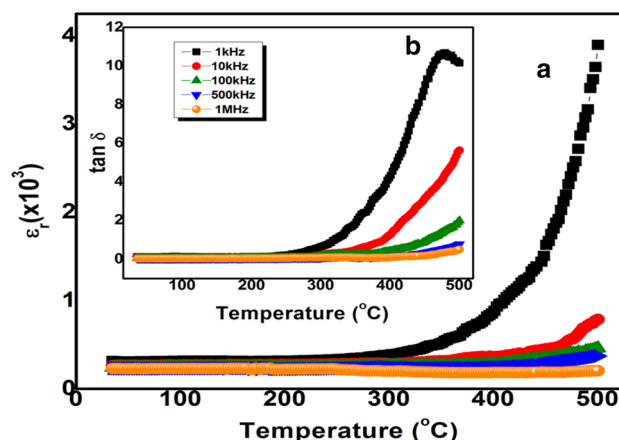


Fig. 3 a, b Variation of relative dielectric constant and tangent with temperature at different frequency

sustain and obey the external field which causes the decrease in polarisation and also there is no charge accumulation at the interface [22]. At low frequencies, dielectric constant and tangent loss do not depend on temperature that may be due to the presence of ion core type of polarization in the sample. However, at high temperatures, they are temperature dependent (i.e., it increases with increase in temperature and decreases with an increase in frequency, which occurs due to the interfacial polarization mechanism). The dielectric constant is larger at higher temperatures and low frequencies that may be due to space charge polarization. It is due to blocking of charge carriers at the electrodes caused by restriction to their motion at the interface [23]. Similarly, we can notice the dielectric dispersion at low frequencies and temperatures [24, 25]. The value of $\tan\delta$ increases slowly at low temperatures, but is relatively sharper at higher temperatures (as shown in Fig. 3b). This trend of variation in $\tan\delta$ at high temperatures occurs due to the presence of some unknown defects (including oxygen vacancies) in the sample that enhances the conductivity/scattering of charge carriers [26, 27].

3.3 Polarization study

The measurement of polarisation is one of the important features of ferroelectrics. Figure 4 displays the room temperature electric field dependence of polarisation (P–E loop) of the compound measured at 100 Hz frequency and a electric field of 2 KV/cm. From the trend of variation of the hysteresis loop, the presence of ferroelectricity in the compound is confirmed. The polarisation loop is more regular that may be due to the reduction of leakage current. The remnant polarization and coercive field of the sample are found to be 0.009 ± 0.001 and 0.76 ± 0.04 respectively.

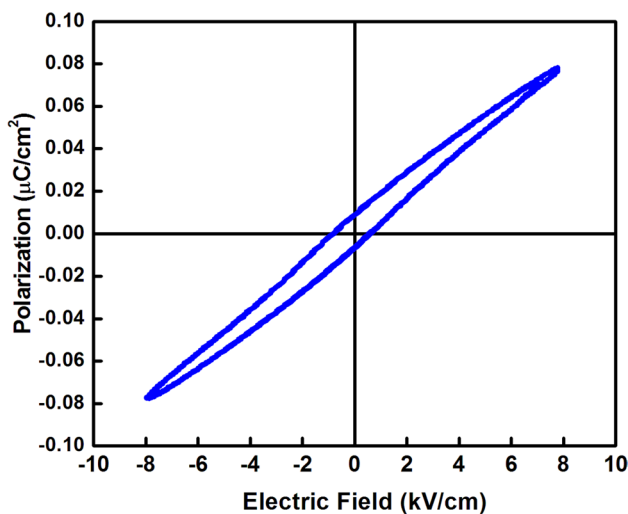


Fig. 4 Polarization with electric field for the compound $(\text{Bi}_{1/2}\text{Li}_{1/2})(\text{Zn}_{1/2}\text{W}_{1/2})\text{O}_3$

3.4 AC conductivity

Electrical conduction in ceramics occurs due to the movement of weakly bound charge particle under the influence of applied electric field. The conductivity study provides information about the transport properties of the compound. The impact of frequency on the electrical properties of the compound can be studied from the analysis of electrical conductivity. The total electrical conductivity (σ_T) of a compound arises due to the ac (σ_{ac}) and dc (σ_{dc}) component of electric field: $\sigma_T = \sigma_{dc} + \sigma_{ac}$. The (σ_{ac}) value is dependent on frequency in the high frequency region whereas it is independent in the low-frequency region. The dc conductivity (σ_{dc}) is a frequency independent part which can be obtained by extrapolating the conductivity graph in the low frequency region [28]. In a perfect dielectric material, when a voltage is applied across the sample, an alternating current ($I = j\omega\epsilon C_0V$) flows through it. On the whole, an in-phase component of current will appear corresponding to a resistive current between the condenser plates which is due to dielectric medium. The ac conductivity of the dielectric can be comprehended from the real part of current density passing through it. The ac conductivity of the sample can be calculated from the dielectric data using the relation given below:

$$\sigma_{ac} = \omega\epsilon\epsilon_0 \tan \delta \quad (1)$$

where ϵ_0 = dielectric permittivity of free space, σ_{ac} is the ac conductivity, angular frequency $\omega = 2\pi f$ (f = frequency), ϵ = relative dielectric constant, $\tan\delta$ = tangent loss. The effect of ac current on the conductivity can be known from the above equation.

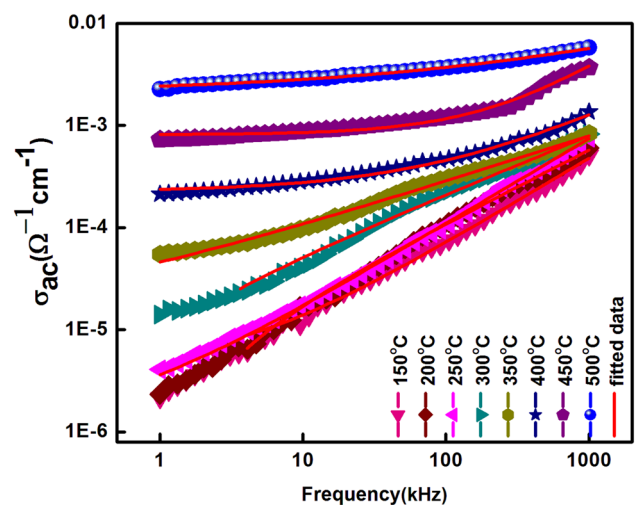


Fig. 5 Variation of ac conductivity with frequency at selected temperature of $(\text{Bi}_{1/2}\text{Li}_{1/2})(\text{Zn}_{1/2}\text{W}_{1/2})\text{O}_3$

The frequency dependence of ac conductivity spectrum of the prepared sample BLZW at different temperatures is displayed in Fig. 5. With the increase in temperature and frequency, the conductivity increases while it decreases with decline in frequency that can be observed in the conductivity pattern. The increasing trend of conductivity may be attributed to disordering of cations between neighbouring sites and presence of conductivity space charges. As the conductivity rises with increase in temperature, the negative temperature coefficient of resistance (NTCR) behaviour of the material is justified.

It can be noticed that the material shows dispersion as in the higher frequency side, the conductivity curves approaches and coincides with each other, and hence this phenomena is known as the low-frequency dispersion [29, 30]. The conduction mechanism of the compound can be better understood by using the universal Jonscher's power law [31].

$$\sigma_T = \sigma_{dc} + A\omega^n \quad (2)$$

Here dc conductivity is σ_{dc} which is a frequency independent term and ac conductivity is σ_{ac} [32] and A (pre-exponential factor) is a constant which is temperature dependent term and n is a frequency independent exponent which has value between 1 and 0 [33]. The degree of interaction between the lattice and mobile ions is signified by n , and strength of polarizability is determined by A . Table 1 shows the value of A and n at selected measuring temperatures. The n factor usually decreases with increase in temperature, while A follows a reverse trend. In the lower frequency side, the conductivity spectrum displays dispersion. In the high-frequency region, the frequency dispersion decreases with increase in temperature till all the curves combines to form

Table 1 The values of A and n at different temperatures of $(\text{Bi}_{1/2}\text{Li}_{1/2})(\text{Zn}_{1/2}\text{W}_{1/2})\text{O}_3$

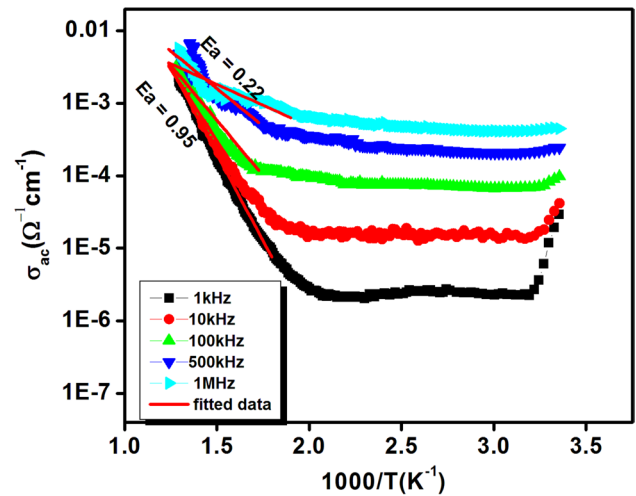
Temperature (°C)	A	n
150	4.0467E-9	0.84499
200	3.2039E-8	0.70941
250	7.4328E-9	0.8333
300	3.1511E-7	0.5675
350	1.4893E-6	0.45339
400	1.2032E-7	0.65661
450	7.4932E-9	0.93445
500	0.00003	0.34682

a single one. From the graph, it can be identified that in the low-frequency region, at high temperatures, the conductivity curves are not dependent on frequency, but at the higher frequency side, it rises with increase in frequency, while reducing the accumulated charges. The reason behind this tendency of curve is the participation of hopping frequency in the conduction mechanism at lower frequency range. This trend of behaviour also justifies that frequency dispersion is still maintained in the compound [34]. Therefore, the dc conductivity can be obtained by extrapolating the lower frequency part. The higher frequency dispersion corresponds to ac conductivity while the frequency independent plateau region is attributed to dc conductivity. The variation of conductivity in the low-frequency side is identified by the effect of polarization at the dielectric interface and electrode. The rise of conductivity at high temperature suggests that the sample have NTCR behaviour. When the n value is < 1 , the hopping of charge carriers involves a translational motion, while for n value higher than 1, the action involves localized hopping without leaving the species in the neighbourhood.

Figure 6 shows the graph of ac conductivity as a function of inverse of absolute temperature at various frequencies. According to Arrhenius relation, at high temperatures, conductivity is expressed as.

$$\sigma_{ac} = \sigma_0 \exp(-E_a/K_B T) \quad (3)$$

where the pre-exponential factor is σ_0 , the Boltzmann constant is K_B and other symbols have their usual meanings that are used to measure the activation energy (E_a) values in different frequency regions. In the plot, there are different slopes for each frequency in different temperature regions. It means the prepared sample has multiple conduction processes with different activation energy [35, 36]. At high temperatures, the conductivity curves for different frequency gets narrowed and seems to merge into a single curve. The release of space charges with increasing temperature is responsible for merging trend of conductivity [37]. From the Arrhenius plots, the different conduction mechanism is noticed in different selected frequency range, and

**Fig. 6** Temperature dependent ac conductivity spectrum of $(\text{Bi}_{1/2}\text{Li}_{1/2})(\text{Zn}_{1/2}\text{W}_{1/2})\text{O}_3$

thus corresponding value of E_a is 0.95, 0.77, 0.62, 0.50 and 0.22 eV for 1, 10, 100, 500 and 1000 kHz respectively. With the increase in temperature and frequency, activation energy of the given sample varies from 0.95 to 0.22 which shows that E_a (activation energy) falls when frequency increases. The reason may be due to the movement of oxygen vacancies of long range type that are contributed in the conduction mechanism [37]. In the studied sample, the conductivity increases as temperature increases, and from the increasing trend of σ_{ac} with the rise in temperature it can be implied that the electrical conduction is a thermally activated process. In the high frequency range, the total conductivity occurs due to restriction of hopping to the neighbouring defect sites while at low frequencies it is due to the hopping/mobility/transportation of charge carriers [38].

3.5 Impedance spectroscopy analysis

The impedance spectroscopic technique is a powerful and robust non-destructive analytic method to study the electrical and dielectric properties of the synthesized specimen, and to examine the response of bulk, grain boundary and electrode on the electrical parameters of the dielectric materials. The temperature and frequency dependent component of impedance Z' (real) and Z'' (imaginary) are calculated using the following basic equations

$$\text{Loss tangent: } \tan \delta = \frac{\epsilon''}{\epsilon'} = \frac{-Z' M''}{Z'' M'} \quad (4)$$

$$\text{Dielectric constant : } \epsilon^* = \epsilon' - j\epsilon'' \quad (5)$$

$$\text{Complex impedance : } Z^* = Z' - Z'' = R_s - \frac{j}{\omega C_s} \quad (6)$$

$$\text{Modulus : } \frac{1}{\epsilon^*} = M^* = M' + jM'' = j\omega C_0 Z^* \times \omega \tag{7}$$

$$\text{Complex admittance : } Y^* = Y' + Y'' = \frac{1}{R_p} + j\omega c_p \tag{8}$$

and

$$Z^2 = Z'^2 - Z''^2 \tag{9}$$

$$M' = -\omega C_0 Z'', \tag{10}$$

$$M'' = \omega C_0 Z' \tag{11}$$

The impedance (Z' and Z'') is described by following equation:

$$Z' = \frac{R}{1 + (\omega\tau)^2} \text{ and } Z'' = \frac{\omega R\tau}{1 + (\omega\tau)^2} \tag{12}$$

where the C_s and R_s are capacitance and resistance in series, the geometrical capacitance is C_o , angular frequency is ω , relaxation time is $\tau = RC$ and other symbols have their usual meanings.

Figure 7 illustrates the frequency variation of Z' and Z'' at different temperatures. The impedance plot shows that the value of Z' declines when both frequency and temperature increase which proves that the given sample shows negative temperature coefficient of resistance (NTCR) behaviour. With increase in temperature, Z' decreases and all the plots completely merge in the high-frequency side to attain an approximate constant value that can be due to semiconductor properties and liberation of space charges at high temperatures [39, 40]. Also, the decrease in Z' with rise in temperature shows the NTCR behaviour of the compound.

The variation of imaginary component of impedance with frequency shows several unique properties, such as: (i) at a

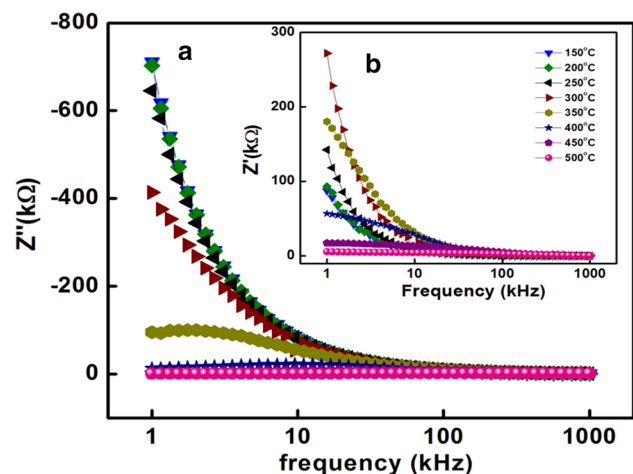


Fig. 7 Complex impedance spectra of $(\text{Bi}_{1/2}\text{Li}_{1/2})(\text{Zn}_{1/2}\text{W}_{1/2})\text{O}_3$ at selected temperatures

distinct frequency the existence of the spectrum peak point (ii) at the region of high frequency complete merging of the impedance spectrum and (iii) with increase in temperature the enhancement in broadening of peak. It can be observed from the plots that with rise in temperature Z'' rises, and by reaching the maximum point (Z''_{max}) it gradually decreases. The Z''_{max} moves to the high-frequency region with the increase in temperature signifying an increase in loss tangent. The asymmetric peak boardening dependent on temperature confirms the presence of multiple relaxation times in the sample. The occurrence of impedance peak shifting with increase in temperature signifies the existence of dielectric relaxation phenomenon because of the relaxation species (vacancies, immobile charges, defects and static charges) which are created in the compound during high temperature processing.

3.6 Nyquist plot

The Nyquist plot is used to analyze the electrical properties due to the grains and grain boundaries by using an electrical network comprising of resistors, capacitors, inductors, capacitors and other distributed circuit elements. The effect of grain, grain boundary and electrode on the resistive behaviour of the specimen can be distinguished from the impedance pattern consisting of one or more semicircles. The variation of impedance [Z' (real) with Z'' (imaginary)] parameters at selected frequency (1 kHz–1 MHz) and temperatures (100–500 °C) is shown in Fig. 8. This plot displays different impedance (capacitive, resistive etc) components that give rise to a series of semicircular curve whose pattern of movement deviates with variation in temperature. In the Nyquist diagram, the number of semicircular arc determines the type of electrical process existing in the compound. All the impedance arc gradually bends to form a semicircle,

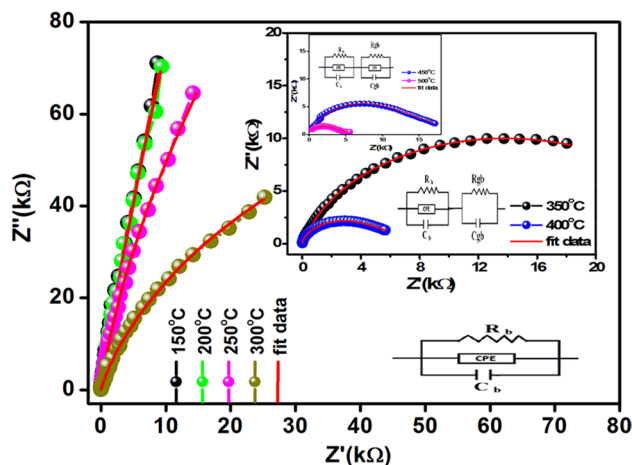


Fig. 8 Variation of Z' with Z'' at different temperature for BLZWO

and appears to have some depression instead of a perfect semicircular arc centred on the real axis with the rise in temperature [29, 41]. The formed semicircle indicates the enhancement in conductivity of the synthesized compound. The existence of a non-Debye type of relaxation mechanism in the compound can be suggested by observing the depressed semicircular arc. The electrical properties of the specimen can be represented by a electrical network comprising of the three elements R (resistance), Q (phase) and C (capacitance). The creation of a singular depressed circular arc at a temperature below 200 °C indicates only the effect of bulk in the compound at this range of temperature, which is fitted using parallel combination of equivalent RQC network. The formation of two semicircular arcs at temperature above 200 °C, (as shown in the insert of Fig. 8) signifies that at the higher temperatures and lower frequencies, the effect of grain boundary contributes in the electrical behaviour of the specimen. From the intercept of the semicircular arcs on the Z' axis, the contribution of grain resistance (R_b) and grain boundary resistance (R_{gb}) to the total resistance of the compound at selected temperatures are estimated and compared in Table 2. The NTCR behavior in the compound can be indicated from the decreasing value of R_b with increase in temperature.

3.7 Electrical modulus analysis

Figure 9a and b shows variation of the modulus [real (M') and imaginary (M'')] spectrum with frequency at selected temperatures. The value of M' approaches to a smaller value (almost zero) at low frequencies, and on increasing temperature the curve of M' tends to increase and coincides with each other at the high frequencies illustrating the nonexistence of electrode polarisation effect in the compound. This nature of the M' occurs due to the existence of conduction phenomenon [42]. The movement of charge carriers of short-range nature proves that for mobility of charges there is a deficiency of restoring force due to the effect of steady electric field [43]. From Fig. 9b, it can be noticed that with rise in temperature

peak of M'' max (relaxation peak) tends to move to high frequency side (i.e., dielectric relaxation is dependent upon temperature) indicating a thermally activated nature of relaxation time. The frequency at which M'' attains a utmost value is called relaxation frequency. As per the detailed analysis of the temperature and frequency dependent impedance and modulus data including role of grain and grain boundaries, and broadening of unsymmetrical M'' peaks, the existence of non-Debye type of relaxation and the distribution of relaxation process with different time constants has been suggested.

3.8 Measurement of magneto–electric coefficient

Magneto–electric (ME) effect refers to mutual coupling of the electric and magnetic properties of the compound. The ME effect is produced in a ferromagnetic material when magnetization induced electric field polarization due to contact between magnetic and electric dipoles and electric field induced magnetization. The ME effect can be present in both composite and single-phase compounds. The ME voltage coefficient usually characterizes the coupling of ME effect. By simultaneous applying of the AC and DC magnetic field, the ME coefficient can be measured by using the following expression [44]:

$$\alpha_{ME} = \frac{dE}{dH} = \frac{1}{d} \frac{dV}{dH} = \frac{V_{out}}{h_0 d} \quad (13)$$

where the magnitude of the ac magnetic field is h_0 , ME voltage is V , the applied magnetic field is H , E is the induced electric field, and d is the thickness of the specimen. To measure the ME effect we have applied 1 kHz frequency and 15.37 Oe AC magnetic fields. The ME set up with lock-in-amplifier has been used to measure the voltage developed across the specimen. The AC current generated by a function generator drives the Helmholtz coil ($N=200$ turns with a radius, $r=2.5$ cm and coil resistance, $R=23.4$). Figure 10 displays the ME coupling coefficient variation with an applied DC magnetic field for the sample BLZWO. Based

Table 2 Fitting parameters of Bulk and grain boundary resistance as well as capacitance of impedance parameters of the compound ($\text{Bi}_{1/2}\text{Li}_{1/2}$) ($\text{Zn}_{1/2}\text{W}_{1/2}$) O_3

Temperature (°C)	Rg (Ω)	Cg (F)	CPE	Rgb (Ω)	Cgb (F)	CPEgb
150	1.000E+020	1.431E−010	5.822E−010	–	–	–
200	7.257E+007	1.202E−010	4.622E−011	–	–	–
250	6.879E+006	1.254E−010	5.107E−010	–	–	–
300	1.812E+006	8.190E−011	1.916E−009	–	–	–
350	2.930E+005	1.398E−10	7.713E−012	3.052E+003	6.417E−010	–
400	6.317E+004	1.640E−010	3.744E−011	6.415E+003	2.654E−008	–
450	1.048E+004	1.574E−010	7.649E−009	9.030E+003	1.000E−025	3.872E−007
500	5.658E+002	1.070E−007	6.833E−013	4.937E+003	1.045E−007	2.064E−007

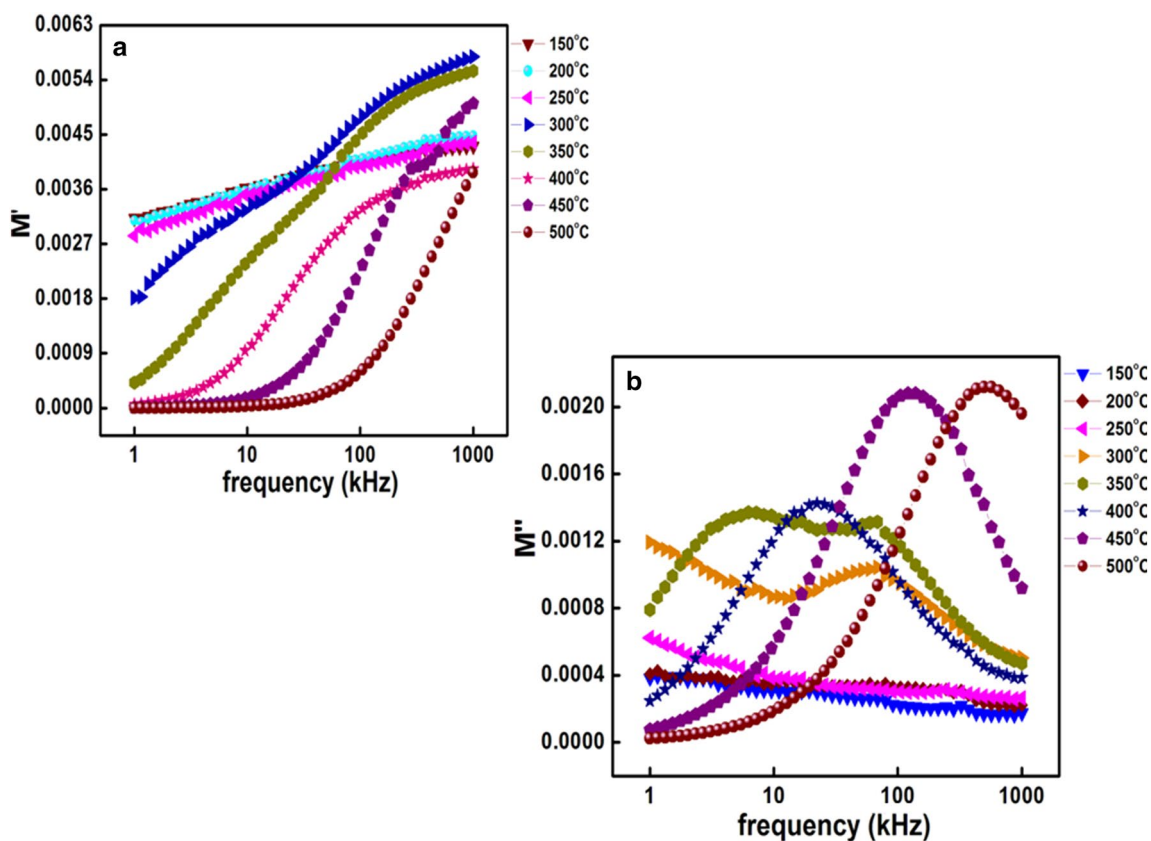


Fig. 9 a–b Variation of complex modulus (real and imaginary) with frequency at different temperature of $(\text{Bi}_{1/2}\text{Li}_{1/2})(\text{Zn}_{1/2}\text{W}_{1/2})\text{O}_3$

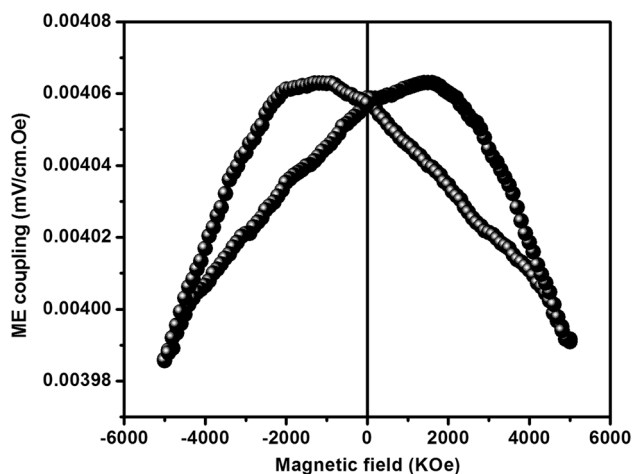


Fig. 10 Room temperature magnetic field dependent ME coupling of $(\text{Bi}_{1/2}\text{Li}_{1/2})(\text{Zn}_{1/2}\text{W}_{1/2})\text{O}_3$

on our experimental data on ME coupling coefficient, the multiferroic characteristics in the prepared compound is confirmed.

4 Conclusion

The BLZWO ceramic is fabricated using a cost effective high temperature solid-state/mixed oxide technique. Analysis of the XRD pattern and data confirms that the fabricated sample have a tetragonal crystal symmetry having 84 ± 0.05 nm crystallite size. A unique flower-like surface morphology is observed (from SEM analysis) of the sintered pellet. The synthesized compound is both frequency and temperature dependent that can be indicated from its electrical properties. The dielectric parameters increase with rise in temperature due to the existence of thermally activated charge carriers in the sample. The prepared compound follows Jonscher's universal power law which can be signified by observing the nature of frequency dependent ac conductivity spectra. From the temperature dependent conductivity plots, it is found that the activation energy of the sample decreases (0.95–0.22) with rise in frequency (1 kHz–1 MHz) that may be due to the movement of oxygen vacancy in the conduction process. Comprehensive analysis of impedance characteristics of the material along with the related parameters of the sample illustrated the existence of grain and grain boundary effects, non-Debye type of relaxation phenomena, subsistence of semiconducting nature (NTCR-type behaviour) in

the prepared sample. In the Nyquist plots, an equivalent circuit has been used to illuminate the electrical phenomenon occurrence inside the synthesized compound. The polarisation electric field (P–E) loop indicates that the sample has a ferroelectric property at room temperature. Modulus analysis shows that the compound has non-exponential conductivity relaxation phenomenon that varies with temperature. The polarization loop and magneto–electric coefficient characteristics affirm the existence of multiferroic nature in the compound.

References

- R.D. Richtmyer, *J. Appl. Phys.* **10**, 391 (1939)
- A.K. Tagantsev, J.W. Lu, S. Stemmer, *Appl. Phys. Lett.* **86**, 032901 (2005)
- S. Bhuyan, K. Sivanand, S.K. Panda, R. Kumar, J. Hu, *IEEE Magn. Lett.* **2**, 6000204 (2011)
- W. Eerenstein, N.D. Mathur, J.F. Scott, *Nat. London* **442**, 759 (2006)
- M.M. Kumar, V.R. Palkar, K. Srinivas, S.V. Suryanarayana, *Appl. Phys. Lett.* **76**, 2764 (2000)
- Y.P. Wang, L. Zhou, M.F. Zhang, X.Y. Chen, J.M. Liu, Z.G. Liu, *Appl. Phys. Lett.* **84**, 1731 (2004)
- K. Asakura, M. Shimomura, T. Shodai, *J. Power.* **119**, 902 (2003)
- T. Xu, W. Wang, M.L. Gordin, D. Wang, D. Choi, *JOM* **62**, 24 (2010)
- S.N. Das, S.K. Pradhan, D.P. Kar, S. Bhuyan, R.N.P. Choudhary, *J. Mater. Sci.: Mater. Electron.* **29**, 9375 (2018)
- A. Fotouhi, D.J. Auger, K. Propp, S. Longo, M. Wild, *Renew. Sust. Energ. Rev.* **56**, 1008 (2016)
- T.H. Kim, J.S. Park, S. Chang, S. Choi, J. Ryu, H.K. Song, *Adv. Energy Mater.* **2**, 860 (2012)
- Q. Zhang, X. Luo, L. Wang, L. Zhang, B. Khalid, J. Gong, H. Wu, *Nano Lett.* **16**, 583 (2016)
- C. Klingshirn, *Phys. Stat. Solidi (b)*, **244**, 3027 (2007)
- S.N. Das, S.K. Pradhan, S. Bhuyan, R.N.P. Choudhary, *J. Mater. Sci.: Mater. Electron.* **28**, 18913 (2017)
- E. Wu, *J. Appl. Cryst.* **22**, 506 (1989)
- K. Parida, S.K. Dehury, R.N.P. Choudhary, *Phys. Lett. A* **380**, 4083 (2016)
- B.D. Cullity, *Elements of X-ray Diffraction* (Addison-Wesley, Reading, 1978)
- R.D. Gould, C.J. Bowler, *Thin Solid Films* **164**, 281 (1988)
- B.B. Ismail, R.D. Gould, *Phys. Status Solidi (a)* **115**, 237 (1989)
- J.B. Moon, A.S. Bhalla, C.B. Chun, K.J. Nam, *Phys. Status Solidi (a)* **140**, 239 (1993)
- S.C. Raghavendra, R.L. Raibagkar, A.B. Kulkarni, *Bull. Mater. Sci.* **25**, 37 (2002)
- S.N. Das, S. Pradhan, S. Bhuyan, R.N.P. Choudhary, P. Das, *J. Electron. Mater.* **46**, 1637 (2017)
- S. Halder, K. Parida, S.N. Das, S.K. Pradhan, S. Bhuyan, R.N.P. Choudhary, *Phys. Lett. A* **382**, 716 (2018)
- J.C. Anderson, *Dielectrics* (Chapman and Hall, London, 1964)
- G.A. Samara, *Solid State Phys.* **18**, 1 (1984)
- S. Halder, S. Bhuyan, S.N. Das, S. Sahoo, R.N.P. Choudhary, P. Das, K. Parida, *Appl. Phys. A* **123**(12), 781 (2017)
- S.N. Das, S.K. Pradhan, S. Bhuyan, S. Sahoo, R.N.P. Choudhary, M.N. Goswami, *J. Electron. Mater.* **47**, 843 (2017)
- S.K. Pradhan, S.N. Das, S. Bhuyan, C. Behera, R.N.P. Choudhary, *J. Mater. Sci.: Mater. Electron.* **28**, 1186 (2017)
- D.P. Almond, A.R. West, *Solid State Ion.* **11**, 57 (1983)
- N.K. Karan, D.K. Pradhan, R. Thomas, B. Natesan, R.S. Katiyar, *Solid State Ion.* **179**, 689 (2008)
- A.K. Jonscher, *Nature* **267**, 673 (1977)
- B. Jimenez, P. Duran-Martin, A. Castro, P. Millan, *Ferroelectrics* **186**, 93 (1996)
- S.K. Pradhan, S.N. Das, S. Halder, S. Bhuyan, R.N.P. Choudhary, *J. Mater. Sci.: Mater. Electron.* **28**, 9627 (2017)
- S.N. Das, A. Pattanaik, S. Kadambini, S. Pradhan, S. Bhuyan, R.N.P. Choudhary, *J. Mater. Sci. Mater. Electron* **27**, 10099 (2016)
- K.K. Mishra, A.T. Satya, A. Bharathi, V. Sivasubramanian, V.R.K. Murthy, A.K. Arora, *J. Appl. Phys.* **110**, 123539 (2011)
- A. Tripathy, S.N. Das, S.K. Pradhan, S. Bhuyan, R.N.P. Choudhary, *J. Mater. Sci.: Mater. Electron.* **29**, 4770 (2018)
- T.L. Qu, Y.G. Zhao, D. Xie, J.P. Shi, Q.P. Chen, T.L. Ren, *Appl. Phys. Lett.* **98**, 173507 (2011)
- S. Bhattacharya, S.S. N.Bharadwaja, S.B. Krupanidhi, *J. Appl. Phys.* **88**, 4294 (2000)
- S. Pattanayak, R.N.P. Choudhary, P.R. Das, *J. Mater. Sci.* **24**, 2767 (2013)
- D.K. Pradhan, B. Behera, P.R. Das, *J. Mater. Sci.* **23**, 779 (2012)
- S. Halder, K. Parida, S.N. Das, S. Bhuyan, R.N.P. Choudhary, *J. Mater. Sci.: Mater. Electron.* **28**, 15928 (2017)
- K. Parida, S.K. Dehury, R.N.P. Choudhary, *J. Mater. Sci.* **27**, 11211 (2016)
- R. Macdonald, *Solid State Ion.* **13**, 147 (1984)
- Y. Zhang, J.P. Zhou, Q. Liu, S. Zhang, C.Y. Deng, *Ceram. Int.* **40**, 5853 (2014)